Mechatronics xxx (2011) xxx–xxx

Contents lists available at ScienceDirect

Mechatronics

journal homepage: www.elsevier.com/locate/mechatronics

The sweep-extend mechanism: A 10-bar mechanism to perform biologically inspired burrowing motions

Robert C. Richardson [c,*], Arjun Nagendran [b], Robin Scott [a]

[a] Oxford Technologies Ltd., Abingdon, Oxon OX14 1RJ, UK
[b] Institute for Simulation and Training, 3100 Technology Pkwy, Orlando, FL 32826, USA
[c] School of Mechanical Engineering, University of Leeds, Leeds, LS2 9JT, UK

ARTICLE INFO

Article history:
Received 3 September 2009
Accepted 13 March 2011
Available online xxxx

Keywords:
Four-bar linkage
Search and rescue
Mechanism
Robot
10-Bar

ABSTRACT

A new type of mechanism has been designed to move an output point through a motion akin to a swimmer's breast-stroke. The mechanism is designed to clear loose debris from around small mobile search and rescue robots. However, it has potential applications in many other domains that require controllable cyclic motion. This paper describes the mechanism concept and presents mathematical analysis of its design parameters. The properties of the mechanism were examined to understand how the mechanism trajectory can be altered mid-cycle whilst maintaining the condition of continually rotating motors. Furthermore, equations to calculate the mechanism torque ratio were derived. The analysis reveals limitations in the trajectory variations that can be implemented whilst maintaining the condition of continually rotating motors. The mechanism was manufactured to validate the mathematical predictions. It was found that the predicted torque ratios are within 90% of the experimentally obtained torque output. The mechanism was controlled using proportional-derivative control (PD) and demonstrated to track several desired trajectories without reversing the direction of motor travel, with tracking error less than ±4 mm.

1. Introduction

Urban search and rescue (USAR) robotics is becoming an increasingly popular research area due to the relatively expendable nature of machines when compared to human or canine searchers. Following a disaster, the majority of human survivors will be in open spaces for rapid extraction by rescue personnel. The greatest challenge for rescue robotics is to penetrate deep within collapsed buildings to search for survivors. Within the debris pile, space is limited and secondary collapse is a real danger to rescuers.

USAR robots deployed into debris piles can easily become overwhelmed by loose debris that accumulates around the robot and restricts motion [1]. Two approaches have been proposed to overcome the problems encountered by loose debris: (i) the design of slender, flexible and dexterous robots (ii) use of manipulators to clear a path.

Snake robots have the potential to wriggle through debris and therefore reach difficult to access areas. Several impressive prototype snake designs have been created [2,3], however snake robot locomotion is complex to create/control and slow (using current technology). It is possible to combine the robustness and speed of tracked robots with some of the dexterity of snake robots [4]. Prof. Hirose's impressive work implemented multiple track modules combined together by active movement of one module relative to another. However, the combination of these two features results in a system too bulky wriggle through a densely cluttered environment.

Many USAR robots are designed to include a manipulator; for example Foster-Miller's Talon robot, Matilda, MARV, Pacbot and Telemax. However, the loose debris in a search and rescue environment presents a significant challenge for conventional pick and place robotic technology; a manipulator would have to be operator controlled or use image processing to pick and place every piece of debris. The time taken for each pick and place operation would preclude deployment of the system.

In this work it is proposed that a mechanism can be designed that will use mechanical properties to remove loose debris and therefore negate the need for external sensors (such as cameras and image processing techniques) and highly dexterous robot manipulators.

Mechanisms are considered largely obsolete for many modern robotic applications due to the availability of high-power-to-weight actuators and digital motor control. However, there are still niche areas where mechanism development is the key to the systems success – these include robotic surgery, prosthetic hands and passive suspension systems.

* Corresponding author.
E-mail addresses: R.C.Richardson@Leeds.ac.uk (R.C. Richardson), Arjun.nagendran@gmail.com (A. Nagendran), robin.scott@oxfordtechnologies.co.uk (R. Scott).

0957-4158/$ - see front matter © 2011 Elsevier Ltd. All rights reserved.
doi:10.1016/j.mechatronics.2011.03.002

Nomenclature

a,b	suffix to denote four bar mechanism a or b
A	rocker rotation point
B	output tip
F	output force at point B normal to line AB (Newtons)
e	extension profile variable
J	joint
$L_1 \ldots L_6$	mechanism link lengths (mm)
L'	four-bar mechanism dynamic link length (mm)
L''	radial distance AB (mm)
M	drive motors
q_d	phase difference between the two rockers (radians)
R	sweep angle (radians)
r_1	global mechanism rotation angle (radians)
r_2	rotation of four bar a with respect to b (radians)
x, y	co-ordinate positions of point B (mm)
w_o	largest workspace radius
w_i	smallest workspace radius
$\theta_{2\min}, \theta_{2\max}$	minimum and maximum output angle (radians)
θ_1	input crank angle (radians)
θ_2	output rocker angle (radians)
θ_3, θ_4	four-bar mechanism angles (radians)
θ_6, θ_7	angles used in inverse kinematics (radians)
θ_5	angle between $L5a$ and $L5b$ radians
$\theta_{2\text{range}}$	movement range of the rocker (radians)
$\theta_{\text{in}(a)}, \theta_{\text{out}(a)}$	four bar angles to calculate force output (radians)
τ_1, τ_2	crank torque and rocker torque respectively (N/m)

Robotic systems have revolutionised surgery by allowing operations to be conducted through small openings, causing less trauma and likelihood of infection. The application of laparoscopic devices through small ports is aided by mechanisms that can specify a limited range of output motion to protect the patient from damage should problems in control occur [5]. Moreover, the mechanisms can allow remote placement of actuators thus allowing easier sterilization of the links and passive pivot points [6]. Intricate motion and multiple degrees of freedom can be achieved within a patient's body by using a laparoscopic device of slender cross-section with mechanisms that allow remote (body-external) actuation. Actuation forces can be transmitted through the instrument by gears [7], cables [8] or pulley/cable arrangements as used within the da Vinci EndoWrist system [9].

Mechanism development can be pivotal in providing dexterous manipulation capabilities. The use of mechanisms in robotic grippers allows large contact forces to be applied via remotely located actuators that are too large and obstructive to be contained 'at-site' [10]. Use of remote actuation in the Robonaut hand has enabled the creation of a device which has the proportions and partial dexterity of the human hand [11].

Mechanism design has been very successful in passive suspension systems. For instance, stringent weight and reliability requirements on Mars missions have resulted in rover suspension systems to be designed as passive in operation [12]. Mechanisms can also be used to locate actuators remotely at a fixed base, thus allowing the mechanism to be potentially very light-weight. This can be used for accurate tip-position with less potential for causing damage to the external environment when compared to heavier mechanisms [13]. Moreover, the mechanism properties can be used to create complex output trajectories from linear motions of the driving actuators [14].

Four-bar linkage systems are a common method of generating oscillatory motion from constant rotation input. These have the advantages of creating complex motion from simple constant rotation and allowing actuators to be positioned away from the moving parts of the system. A simple 5 bar linkage has been used to create a robot to pick fruit [15]. This demonstrated improved dynamic performance over conventional serial link manipulators due to remote centre of operation. Zhixing et al. [16] present a method for designing the lengths of a four bar mechanism and developed software to automate the process. These properties can also be analysed through an algebraic approach [17].

The novel servo controlled mechanism discussed in this paper creates output trajectories from two remotely positioned motors rotating in one direction only. The mechanism is capable of a combined circumferential forward/backward motion (sweep) and radial extension/retraction motion.

The robot concept is illustrated in Fig. 1. Two external manipulators protrude from the robot body to manipulate external debris [18].

The end effectors are required to move small, loose debris from the front of the robot to the side through the use of two independent arms. Therefore, there is a requirement for each arm to move through the motion as illustrated in Fig. 2. This motion is based around biological inspiration of the European mole as discussed in previous work [19]. The motion can be split into discrete stages with sweep used to describe the circumferential motion. It is important that the motion can be varied between cycles or even during a cycle depending upon the current external conditions.

The research objective of this work is to create a mechanism that can move an output tip through cyclic motions as indicated in Fig. 2, whilst satisfying the following criteria: (i) the extension/retraction can be altered during the motion (ii) the actuators are located away from the mechanical links and output tip (remote centre of operation) to protect them from damage in harsh environments and allow the actuators to remain in a fixed position relative to the body, (iii) the actuators continually move in the same direction to minimise backlash effects in the motor and achieve better efficiency (motors are far more efficient running in a single direction within velocity bounds) (iv) Force requirement: The mechanism should minimise scaling of the input torque from the motors with respect to the output torque.

The rest of the paper is organised as follows. Section 2 describes the conceptual design and mechanism theory including analysis of

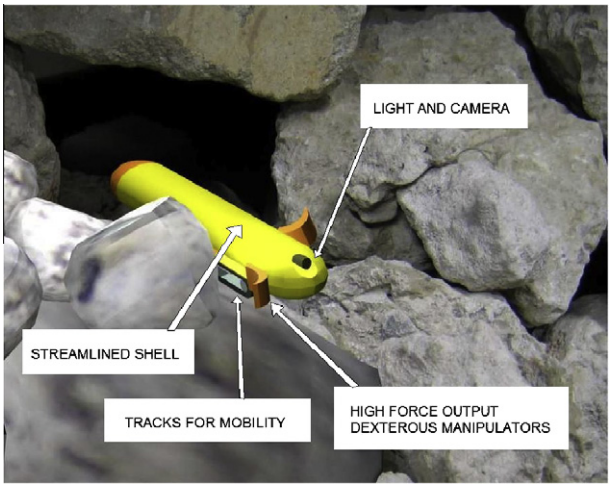

Fig. 1. Robot concept.

Please cite this article in press as: Richardson RC et al. The sweep-extend mechanism: A 10-bar mechanism to perform biologically inspired burrowing motions. Mechatronics (2011), doi:10.1016/j.mechatronics.2011.03.002

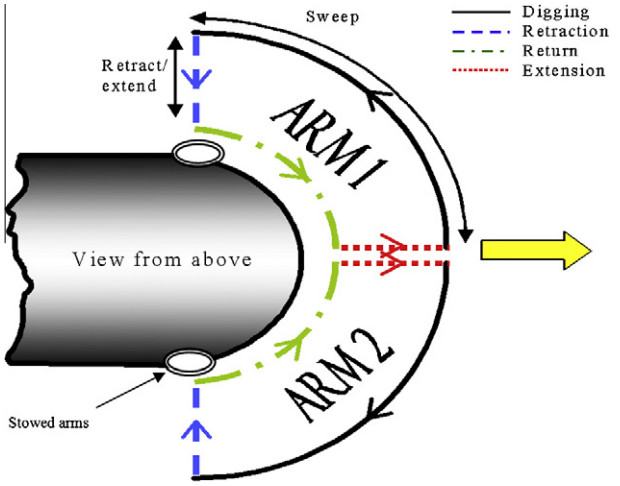

Fig. 2. Biologically inspired digging trajectory showing digging stages.

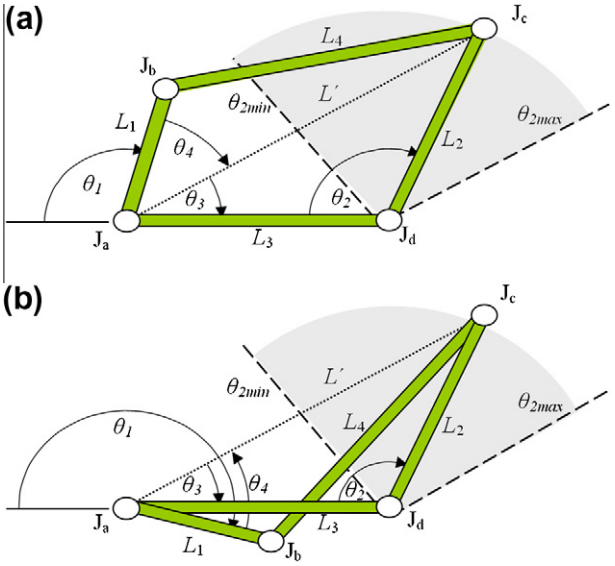

Fig. 3. Four-bar mechanism in (a) positive and (b) negative positions.

the mechanism parameter selection and output torque. Section 3 considers the dimensional analysis including describing the experimental hardware measurement of the mechanism torque ratio and trajectory tracking performance. Section 4 discusses the key points of the work and finally Section 5 draws conclusions.

2. Conceptual design and mechanism theory

There are many mechanisms described in the literature that produce complex movement from continuous rotation, for example: [20] Swing-arm quick return mechanisms that use a constant input rotation to produce a linear motion with different speeds for extension and retraction; geared 5 bar mechanisms that use a combination of multiple links and gears around the crank; and treadle drive mechanisms that are used for moving sewing needles and driving grinding wheels. However, these mechanisms often require sliders or gears close to the output tip which is very undesirable in harsh environments. Furthermore, they move a tip through a predefined path that cannot be deviated from during motion.

In a robotic context, the simplest method of implementing a motion that can vary the extension or retraction is to use a conventional two-jointed servo controlled robot arm. This approach requires the actuators to continually change direction and be exposed to harsh conditions. It is possible to use additional mechanical links to mount the actuators at the base of the joint [21], however the motors are still required to continually change direction which is wasteful of energy and places extra wear on the motors, joints and structure.

It is possible to add a servo controlled prismatic joint (linear extending) to the cyclic motion of a conventional mechanism. However prismatic joints provide small amounts of strain (typically around 60%), and they are notoriously vulnerable to damage from dust, dirt and side loads.

A combination of two four bar mechanisms is proposed to produce the required output motion. Consider the Grashof crank-rocker four-bar mechanism [20] shown in Fig. 3a. A continuous rotation of link 1 (L_1) around joint J_a (the crank) results in link 2 rocking backwards and forwards around joint J_d (the rocker). The relative lengths of the links determine the type of four bar mechanism; for a crank-rocker configuration the lengths must meet the following criteria ($L_1 + L_4 < L_2 + L_3$).

A second four-bar mechanism is combined with the first to have a coincident joint J_d, but to be rotated from the first four-bar by an angle r_2 (Fig. 4). Note that from now on the subscript (a) is used to identify parameters on the first four-bar linkage and the subscript (b) for the second four-bar linkage. When subscripts are not used, the variable refers to parameters on both four-bar linkages. The motors M_a and M_b apply input torque to rotate the joints (J_{aa} and J_{ab}) respectively. Joint J_c remains at a distance L_2 from joint J_d but the end of the L_2 is now extended to the overall length L_5 on both mechanisms. The output of both four-bar mechanisms are combined through two additional links L_{6a} and L_{6b} connected to joints of links L_{5a}, L_{5b} at J_{ea}, J_{eb}. L_{6a} and L_{6b} are joined at joint J_f. The crank angles (θ_{1a} and θ_{1b}) and rocker angles (θ_{2a} and θ_{2b}) are measured with respect to a line along link L_{3a} and L_{3b} respectively. The whole mechanism is rotated by an angle (r_1) to align its extension with the horizontal plane (this has no effect on the mechanism, only altering its orientation). The Motors rotate in the opposite direction to the measured angle to use positive four-bar link configurations while performing the sweep action (maximum extension); this results in a torque ratio close to one during the motion.

Fig. 5 illustrates the mechanism output at key points: Fig. 5a shows the tip at maximum extension, with line AB in the horizontal position (facing forward). The two rockers are aligned and the twin four-bar are in positive configurations to provide the greatest output torque. This is the start of the sweep phase. In Fig. 5b the rockers have remained aligned and the line AB is now in the vertical direction. Four-bar b is at the point where the rocker reverses its direction. The rocker of four-bar a will continue in the same direction. This is the start of the retract phase. In Fig. 5c the rockers are now at maximum separation. Four-bar mechanism a is now at the point of reversing the rocker direction, whilst the rocker of four-bar *b* continues in the same direction. This is the start of the return phase. In Fig. 5d the mechanism is now retracted and the AB is aligned with the horizontal plane. Four-bar b is at the point of reversing its rocker, while the rocker of four-bar a will continue in the same direction. This is the start of the extend phase.

2.1. Mechanism parameter selection

The motion shown in Fig. 5 is achieved by maintaining a constant phase difference between the rocker angles (θ_{2a} and θ_{2b}) during mechanism activation. The variable q_d is used to represent the phase difference. Note that q_d is the magnitude of the angle difference as the subtraction of angles become negative due to the rocker backward and forward motion and the sign convention.

$$q_d = |\theta_{2b} - \theta_{2a}| \quad (1)$$

Please cite this article in press as: Richardson RC et al. The sweep-extend mechanism: A 10-bar mechanism to perform biologically inspired burrowing motions. Mechatronics (2011), doi:10.1016/j.mechatronics.2011.03.002

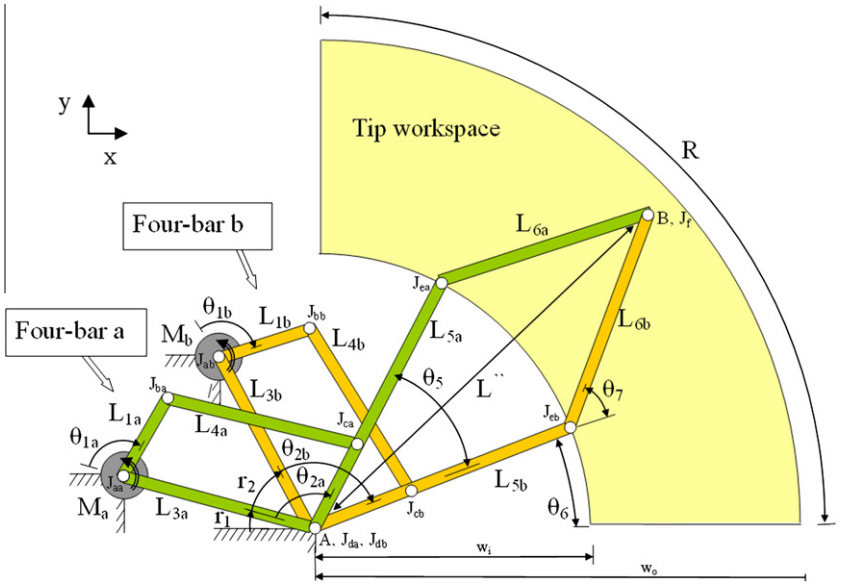

Fig. 4. The mechanism configuration and parameters.

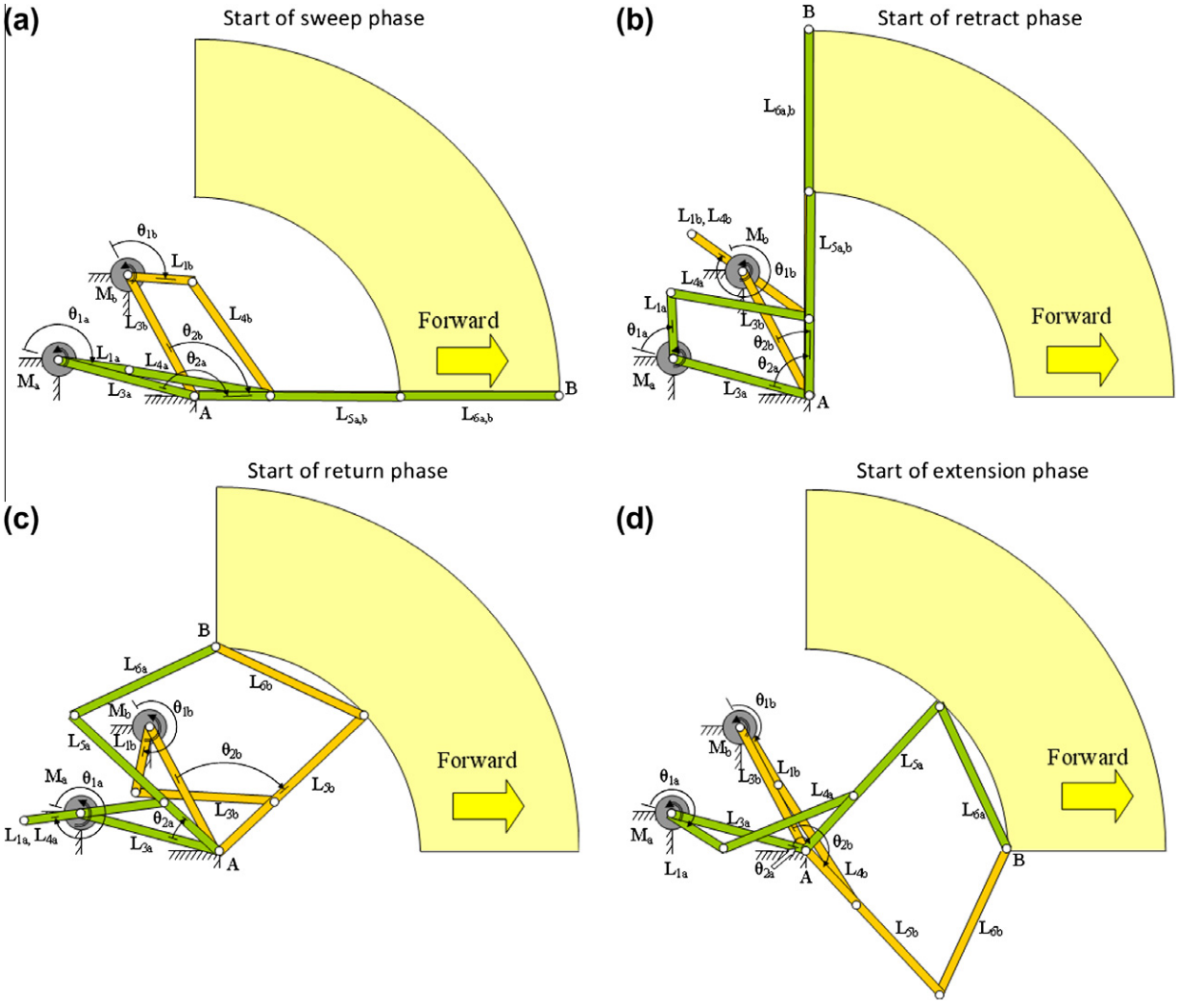

Fig. 5. Link positions for workspace key points.

Please cite this article in press as: Richardson RC et al. The sweep-extend mechanism: A 10-bar mechanism to perform biologically inspired burrowing motions. Mechatronics (2011), doi:10.1016/j.mechatronics.2011.03.002

The value of q_d is not obvious from the figures – the rockers can be overlapped and also at their maximum separation for the same value of q_d. This is due to the measurement of the rocker angles relative to the orientation of each four-bar and not a global reference point. To achieve a constant phase difference each four-bar needs to be servo controlled at the input crank to regulate velocity, whilst maintaining the same direction of motion.

The mechanism is designed to have a workspace at the output tip as shown in Fig. 4. The variables that define this workspace are the outer radius (w_o), the inner radius (w_i) and the angular sweep (R).

When L_{5a} and L_{5b}, and L_{6a} and L_{6b} overlap the tip (B) is on the outer radius. Therefore,

$$w_0 = L_5 + L_6 \tag{2}$$

It is desirable that L_5 does not protrude into the workspace for ease of manufacture and dirt shielding ($L_5 \leqslant w_i$). Conversely, it is desirable that the link L_5 is as large as possible to maximise the extension change for a given change in relative rocker position. Therefore, here $L_5 = w_{i,}$ and $L_6 = w_o - w_{i.}$

The maximum required separation of the links L_{5a} and L_{5b} ($\theta_{5\max}$) can be calculated so that the output tip lies along the w_i line at this maximum separation (Fig. 6). At the maximum separation, the following relationship can be obtained from trigonometry (Fig. 6).

$$L_5 \sin(\theta_{5\max}/4) = \frac{L_6}{2} \tag{3}$$

Therefore, $\theta_{5\max}$ can be calculated by rearranging Eq. (3).

$$\theta_{5\max} = 4 \cdot \sin^{-1}\left(\frac{L_6}{2 \cdot L_5}\right) \tag{4}$$

The four-bar b is rotated around the point A, relative to four-bar A, by $r_2 = \theta_{5\max}/2$ to remove the requirement for links L_{5a} and L_{5b} to cross during motion. This makes the mechanical construction and control more straightforward.

One of the key features of the mechanism is the required range of θ_2 for each four-bar. Considering the motion shown in Fig. 5, the range of angle θ_2 is required to be greater than R at the extremes of motion. If $\theta_{2\min}$ and $\theta_{2\max}$ are the minimum and maximum values of four-bar rocker motion, then the following is true (the rocker can move $\theta_{5\max}/2$ past the horizontal or vertical line of the workspace)

$$R + \frac{\theta_{5\max}}{2} = \theta_{2\max} - \theta_{2\min} = \theta_{2\text{range}} \tag{5}$$

Therefore, the four-bars must be designed have a movement range of $\theta_{2\text{range}}$ for the mechanism to be capable of the required workspace. It is desirable for $\theta_{2\text{range}}$ to be as large as possible to create the largest output workspace, but in practice there is a trade-off between sweep angle and the mechanical advantage; poor design will cause stalling of the system (a torque reduction so great that friction or load affects prevent motion).

A large rocker angle range occurs when links L_1 and L_2 are similar lengths as are links L_3 and L_4 whilst adhering to the Grashof criteria. If operating close to the Grashof criteria threshold, it is important to include margin of error to account for link length tolerances, looseness in the joints and any deflection in the links. It is also important to design a mechanism with transmission angle (the angle between links L_2 and L_4) as close to 90° over the cycle to maximise the transmission of force. There are many formal optimisation techniques available in the literature to assist in the design of four-bars. In this case the techniques developed by Columbia University were used to identify appropriate link length proportions [20]. The technique uses the rocker angle and corresponding crank input angle to identify equations that can be solved through numerical iteration. Once the ratio of link lengths are been obtained they are scaled by one link of known physical desired length (this is normally the crank).

It is interesting to examine the properties of the overall mechanism. Based upon the assumptions above, rearranging Eqs. (2) and (5) and substituting for $\theta_{5\max}$ in Eq. (5) results in the following relationship between the ratio of L_5/L_6 and the sweep angle (R):

$$\frac{L_5}{L_6} = \frac{1}{2 \cdot \sin\left(\frac{2 \cdot (\theta_{2\text{range}} - R)}{4}\right)} \tag{6}$$

If R is increased, the ratio of L_5/L_6 must reduce, resulting in the profiles shown in Fig. 7. There is a clear trade-off between these parameters, with small increases in sweep angle R beyond original design, drastically reducing the workspace width ($w_o - w_i$).

2.2. Output torque

The mechanism torque output is a function of the torque created by the twin four-bars and the kinematic configuration of links L_5 and L_6. The configuration of each four-bar alters the amount of the torque transmitted from the crank to the rocker (Fig. 8). Considering four-bar mechanism (a), the torque applied by link L_{1a} is resolved to a force (F_1) along link L_{4a} at an angle of $\theta_{\text{in}(a)}$ and then resolved normal to link L_{2a} through an angle $\theta_{\text{out}(a)}$ at point J_{ca}. The force (F_2) applied to joint J_{ca} results in a torque around point J_d on L_{2a}. The link 2 torque is the transmitted torque from the four-bar.

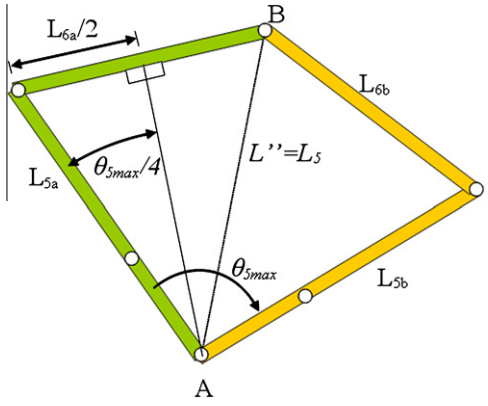

Fig. 6. Calculating link L6 length.

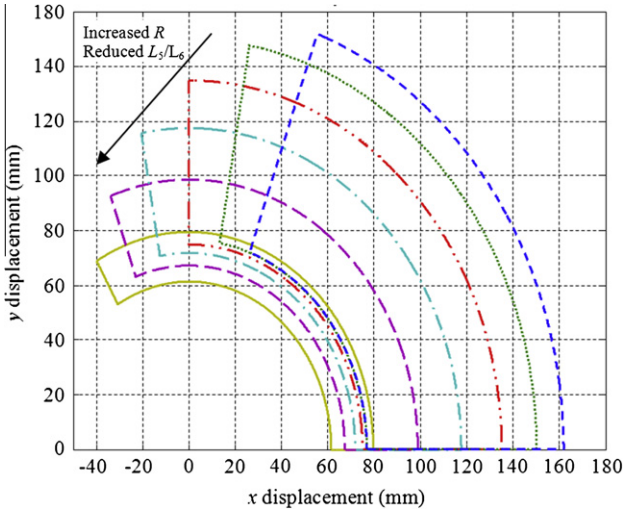

Fig. 7. Sweep vs. extension range.

Please cite this article in press as: Richardson RC et al. The sweep-extend mechanism: A 10-bar mechanism to perform biologically inspired burrowing motions. Mechatronics (2011), doi:10.1016/j.mechatronics.2011.03.002

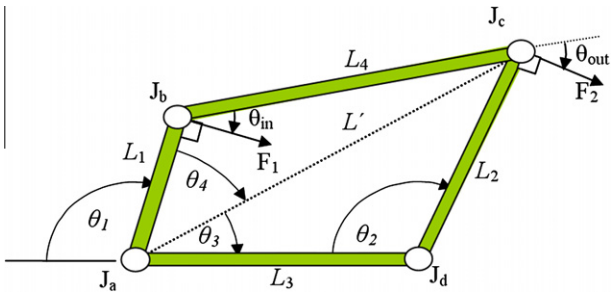

Fig. 8. Calculating the transmitted torque.

Eqs. (7) and (8) find the relevant input and output angles and Eq. (9) gives the torque output. The same equations can be used for four-bar (b) using the relevant subscript.

$$\theta_{\text{in}(a)} = \frac{\pi}{2} - \sin^{-1}\left(\frac{L'_a \sin\theta_{4a}}{L_{4a}}\right) \tag{7}$$

$$\theta_{\text{out}(a)} = \frac{\pi}{2} - \theta_{\text{in}(a)} - \theta_{4a} \tag{8}$$

$$\tau_{2a} = \frac{L_{2a}}{L_{1a}} \cdot \tau_{1a} \cos(\theta_{\text{in}(a)}) \cdot \cos(\theta_{\text{out}(a)}) \tag{9}$$

Eq. (9) reveals the torque on the rocker for a given torque at the crank. The ratio L_{2a} to L_{1a} fundamentally limits the torque that can be transmitted and the angles $\theta_{\text{in}(a)}$ and $\theta_{\text{out}(a)}$ determine how the output torque varies dependant on the four bar configuration.

Eq. (9) can be rearranged to find the torque ratio (output torque divided by input torque) for each four-bar.

$$\frac{\tau_{2a}}{\tau_{1a}} = \frac{L_{2a}}{L_{1a}} \cdot \cos(\theta_{\text{in}(a)}) \cdot \cos(\theta_{\text{out}(a)}) \tag{10}$$

Therefore, for the mechanism to have a torque ratio close to unity, the links L_{1a} and L_{2a} must be similar lengths and the angles $\theta_{\text{in}(a)}$ & $\theta_{\text{out}(b)}$ must be close to zero (L_{4a} normal to L_{1a} and L_{2a}).

For the overall mechanism (Fig. 4), the torques from the four-bars are combined into a force at point B over the length L''. Eq. (11) defines the mechanism torque ratio (the output torque divided by the input torque). The equations that define the mechanism and force under quasi-static conditions are given by Eqs. (12) and (13):

$$\frac{\tau_{2a} + \tau_{2b}}{\tau_{1a} + \tau_{1b}} = \frac{L_{2a}}{L_{1a}} \cdot \cos(\theta_{\text{in}(a)}) \cdot \cos(\theta_{\text{out}(a)}) + \frac{L_{2b}}{L_{2a}} . \cos(\theta_{\text{in}(b)}) . \cos(\theta_{\text{out}(b)}) \tag{11}$$

$$F = L'' \cdot (\tau_{2a} + \tau_{2b}) \tag{12}$$

where

$$L'' = \sqrt{(L_{5a} \sin(q_d/2)^2) - L_{6a}^2} \tag{13}$$

Note that the inverse of the velocity profile is often considered to be the torque output [22]. However, this method calculates the output torque required to stop the input crank and therefore, incorrectly predicts the torque that the rocker can apply (including predicting infinite values of output torque for some angles of crank input).

2.3. Alteration of movement trajectory

The mechanism is intended to operate at its full retracted/extended range for normal operation. However, there will be situations where the extend range will need to be reduced during motion (for example, to avoid immovable objects). The trajectory can be altered by using a different phase difference (i.e. altering q_d). Fig. 9 illustrates the workspace for several values. As the phase difference is reduced the trajectory becomes longer and thinner until at zero phase difference the workspace is reduced to a line. Fig. 4 illustrates the mechanism in the zero phase difference pose (zero phase difference means the four-bars have the same pose relative to their rotation).

Conventional servo control of the cranks enables the tip to move through any profile trajectory. With reference to Fig. 4, the kinematics of mechanism from point A to B can be likened to a standard 2 degree-of-freedom planar manipulator (considering links L_{5b} and L_{6b} as links of the planar manipulator) and as such the standard inverse kinematics solution can be applied as shown in Eq. (14) [23]. In this case the (b) suffix mechanism is used, however either (a) and (b) could be used to obtain the inverse kinematics, if the correct arctan2 solution is used.

$$\theta_6 = \arccos\left(\frac{x^2 + y^2 - L_{5b}^2 - L_{6b}^2}{2 \cdot L_{5b} \cdot L_{6b}}\right) \tag{14}$$

$$\theta_7 = \arctan 2(y, x) - \arctan 2(L_{6b} \sin\theta_6, L_{5b} + L_{6b} \cos\theta_6) \tag{15}$$

From these angles, the necessary rocker angles θ_{2a} and θ_{2b} can be calculated as shown in Eqs. (16) and (17).

$$\theta_{2b} = \pi - r_1 - r_2 - \theta_6 \tag{16}$$

As θ_6 and θ_7 are known, L'' can be calculated from the cosine rule:

$$L'' = \sqrt{L_{5b}^2 + L_{6b}^2 - 2 \cdot L_{5b} \cdot L_{6b} \cdot \cos(\pi - \theta_7)} = \sqrt{L_{5b}^2 + L_{6b}^2 + 2 \cdot L_{5b} \cdot L_{6b} \cdot \cos(\theta_7)} \tag{17}$$

Using the sine rule:

$$\theta_5 = \sin^{-1}\left(\frac{L_{6b} \cdot \sin L''}{\pi - \theta_7}\right) \tag{18}$$

Therefore,

$$\theta_{2a} = \pi - r_1 - \theta_6 - \theta_5 \tag{19}$$

To find respective crank angle, first the length L' is calculated for each four-bar (a or b subscript is dropped here for clarity).

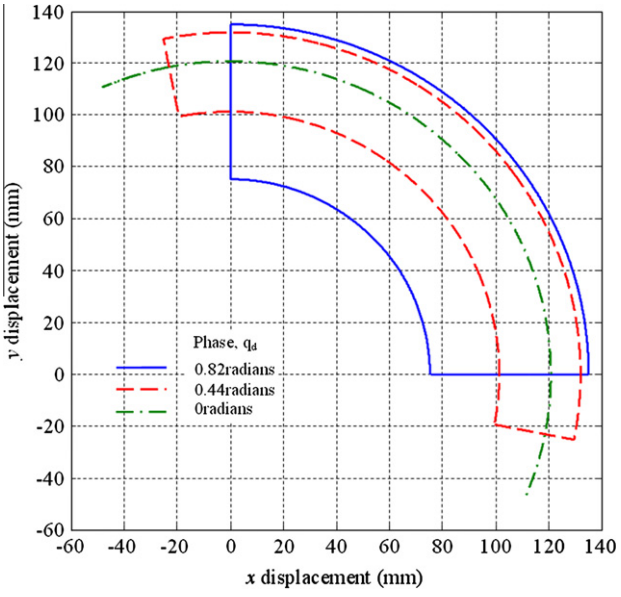

Fig. 9. Trajectory ellipses for varying motor phase values.

Please cite this article in press as: Richardson RC et al. The sweep-extend mechanism: A 10-bar mechanism to perform biologically inspired burrowing motions. Mechatronics (2011), doi:10.1016/j.mechatronics.2011.03.002

$$L' = \sqrt{L_2^2 + L_3^2 - 2 \cdot L_2 \cdot L_3 \cdot \cos\theta_2} \tag{20}$$

L' is then used to find the angles:

$$\theta_3 = \arcsin\left(\frac{L_2 \sin\theta_2}{L'}\right) \tag{21}$$

$$\theta_4 = \arccos\left(\frac{L'^2 + L_1^2 - L_4^2}{2 \cdot L' \cdot L_1}\right) \tag{22}$$

$$\theta_1 = \pi + (\theta_3 \pm \theta_4) \tag{23}$$

Notice here the use of the ± symbol to represent the two possible crank positions.

It is desirable that the cranks do not reverse direction; therefore implementation of movement profiles requires careful consideration. At any given pose the most severe manoeuvre (short of reversing) is to stop the movement of one motor while the other continues. For example, consider the poses illustrated in Fig. 4 for anti-clockwise trajectory with motor (b) stationary, while motor (a) in motion. The tip (B) would then move in an arc around the current position of joint J_{eb} at a radius of L_{6b}.

Consider the anti-clockwise profiles through the workspace illustrated in Fig. 10. Trajectories 2 and 4 cannot be implemented without changing a motor direction (the ratio of sweep motion to extend/retract motion is too low). Trajectories 1 and 3 are valid, with a sufficiently high ratio of sweep motion to extend/retract motion. Note trajectory 3 follows a path of radius L_6 for awhile, this implies one motor has stopped moving.

The edges of motion (at zero horizontal or vertical coordinates) are a special case due to the fact that one rocker has reversed direction allowing for the horizontal or vertical motion without reversing the crank direction. However, problems can be encountered at these regions if the original workspace is deviated from. The rocker has to travel to its minimum/maximum position to reverse direction, placing further restrictions on valid motions.

If the phase difference is altered in the extend/retract phase then is it possible to overcome these issues. At the commencement of the extend phase (when the first rocker reaches its minimum value) a variable e is introduced to scale the phase difference (Eq. (24))

$$\theta_{2a} = \theta_{2b} - e \cdot q_d \tag{24}$$

Varying the value of e within the range [1–0] results in a curved response during the extension or retraction part of the sequence. As e is decreased the extend/retraction stage becomes curved and finishes at new angles and extensions (Fig. 11). Therefore, it is possible to vary extension, whilst maintaining the retracted length. Fig. 12 illustrates two trajectories with reduced extension range and Fig. 13 illustrates the kinematic configuration at these regions.

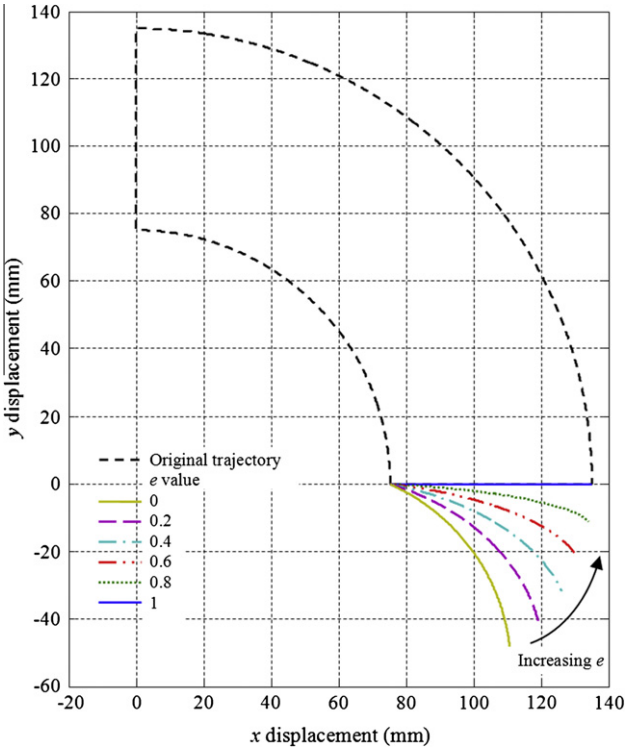

Fig. 11. Altered extension profiles.

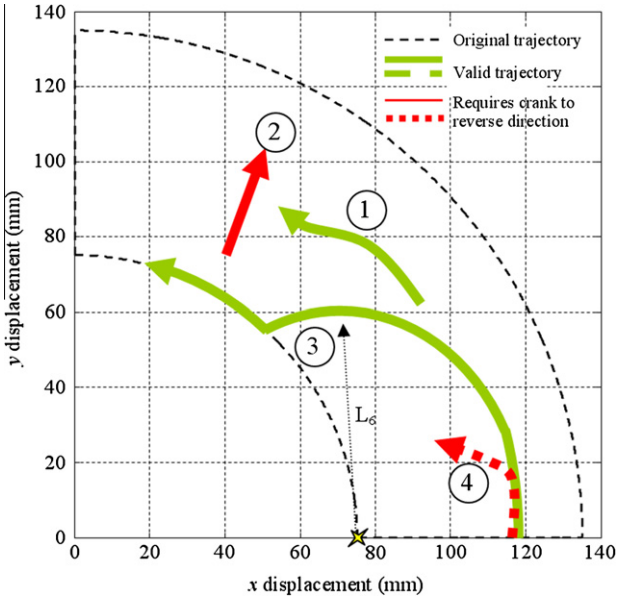

Fig. 10. Valid trajectory paths.

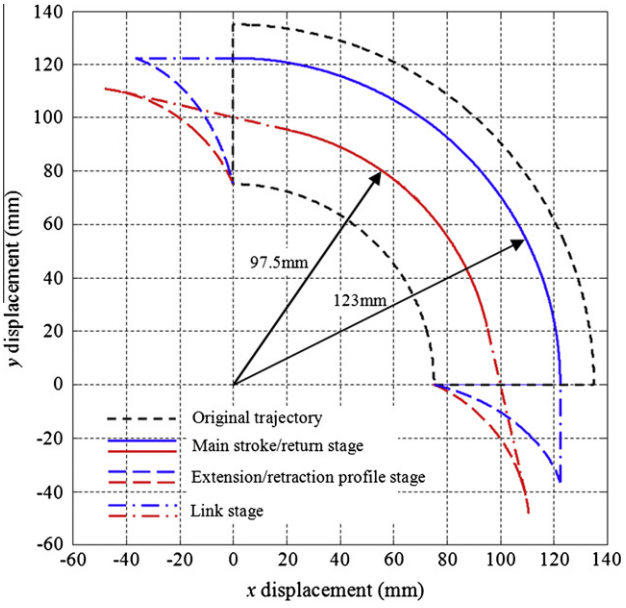

Fig. 12. Blended trajectory.

Please cite this article in press as: Richardson RC et al. The sweep-extend mechanism: A 10-bar mechanism to perform biologically inspired burrowing motions. Mechatronics (2011), doi:10.1016/j.mechatronics.2011.03.002

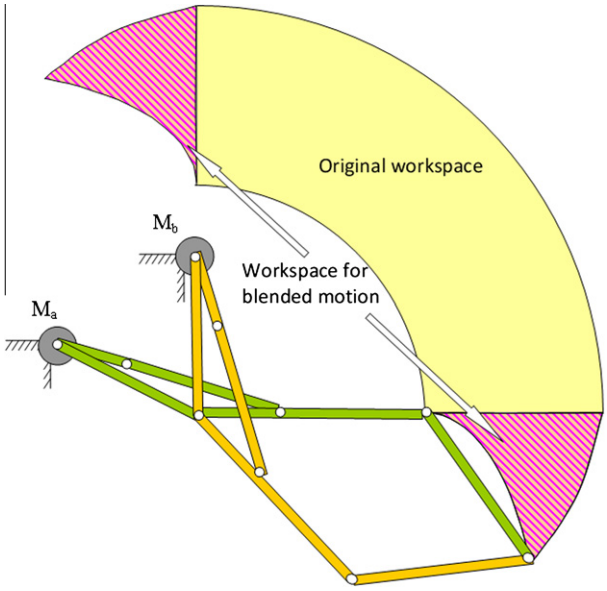

Fig. 13. Modified workspace and mechanism configuration for blended motion.

It should be noted that if the cranks are allowed to reverse direction, then any movement profile is possible. This maybe useful in unusual circumstances, such as when the arm is caught on an immovable object.

2.4. Velocity planning

The mechanism global velocity profile can be directly specified as an *x* and *y* demand position against time and controlled through the motion of the cranks. The movement profile can be specified as the tip having constant magnitude of velocity, constant angular velocity during the sweep and return stages of motion or any combination of profiles. The limit to maximum velocity is dependant upon the input motor torque and the sampling time of the digital controller. In this application, constant angular velocity was selected for the sweep and return stages of motion. The global velocity during the blended motion segments is a result of constant crank rotation, but could be specified to have specific global velocities, if required.

3. Dimensional analysis

Link length values were selected for the experimentally constructed sweep-extend mechanism using the analysis of Section 2. The desired workspace parameters were $w_i = 75$ mm, $w_o = 60$ mm with a sweep angle of $R = 90°$. Therefore, lengths $L_5 = 75$ mm and $L_6 = 60$ mm. The minimum ($\theta_{2\min}$) and maximum ($\theta_{2\max}$) output rocker angle of the four bar linkages can be calculated to be 26.26° and 164.35° respectively resulting in an output rocker range ($\theta_{2\text{range}}$) of 137.09°. The physical size of the motors/gearboxes and space for the mechanism to operate, resulted in a crank length (L_1) = 25 mm and the fixed length (L_3) = 52 mm. The remaining lengths were then calculated as using the four-bar design process [20] resulting in $L_2 = 27$ mm, $L_4 = 52$ mm. These lengths are sub-optimal but provide the correct movement range and acceptable performance (as described in Section 3.2).

3.1. Experimental hardware

Fig. 14 shows the final experimental system constructed using two arms actuated by sweep-extend mechanisms. The shaded area illustrates the output workspace that a single arm can move through. Each constituent four-bar mechanism is driven by a pair of Maxon A-max 32 mm diameter 15 W DC motors through both a Maxon 66.2:1 32 mm diameter Planetary Gearbox and an Ondrives E20 1:1 Crossed Axis Helical Gearbox (to change the axis of rotation). Connected to the motors are Maxon HEDL 5540 3 channel optical encoders used for position measurement along with continuous rotation potentiometers to set the initial angular position. All other mechanical hardware components were designed and custom made for the application. Each arm also contains a 'blade' mounted on linear slides. The linear slides guide the blade to lie

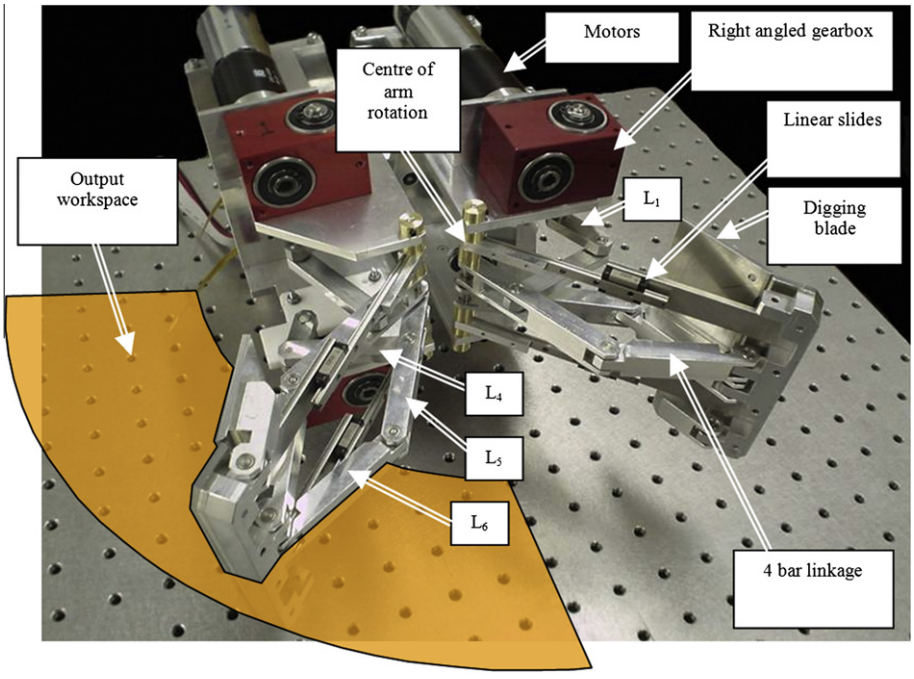

Fig. 14. Mechanism on fixed base.

Please cite this article in press as: Richardson RC et al. The sweep-extend mechanism: A 10-bar mechanism to perform biologically inspired burrowing motions. Mechatronics (2011), doi:10.1016/j.mechatronics.2011.03.002

along the L'' line so that normal forces can be applied – this is a specific addition for this robot application and does not affect the sweep-extend mechanism. A Measurement Computing PCI-QUAD04 4 channel quadrature encoder board is used to read the signals from the optical encoders. As well as this an Eagle Technology PCI-766-16 16 analogue output board and PCI-730-E 16 analogue input board are utilised. These boards are interfaced with National Instruments Labview 7.1 to allow control to be implemented.

3.2. Mechanism torque output

At any given point within the mechanism workspace the tip x and y coordinates are known. Inverse kinematics can be performed on the tip coordinates to find rocker angles (θ_{2a}, θ_{2b}) [Eqs. (14)–(23)]. The mechanism torque ratio can then be found for this these specific coordinates [Eq. (11)]. This process can be repeated for coordinates across the mechanism workspace resulting in torque ration graphs (Figs. 15 and 16).

The torque ratio graphs illustrate that greater torques can be produced in the positive four-bar mechanism mode (Fig. 3a) than in the negative (Fig. 3b), however both modes have torque ratio's no greater than 1 and no smaller than 0.3, with the lower ratios at the corners. It is important to ensure that high torque load regions occur where the four-bar mechanism are operating in the positive position. The low torque ratio operation mode should be reserved for low load regions. For this application the high torque section is designed to be when moving debris from the front of the robot to the side and the low torque section is the no load return stroke action.

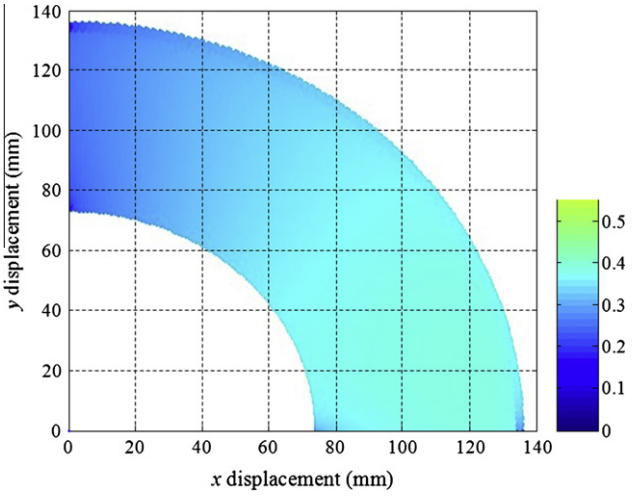

Fig. 15. Torque ratio (negative four-bar mechanism positions).

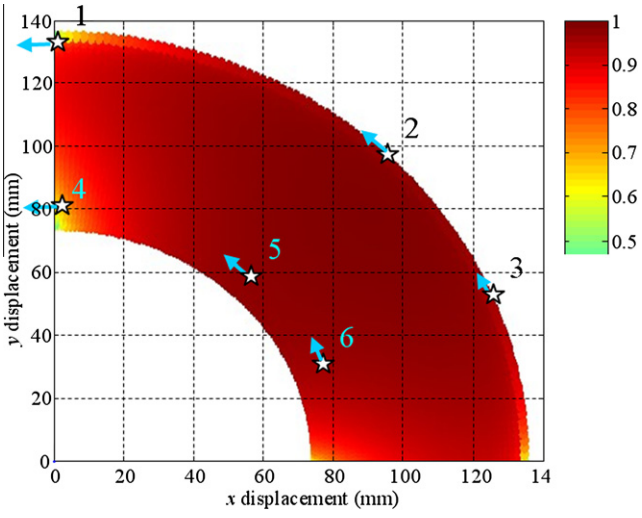

Fig. 16. Torque ratio (positive four-bar mechanism positions).

3.2.1. Experimentally measured output torque

Experiments were performed to determine the torque ratio of the physical mechanism to validate the equations and determine the effect of friction in gearboxes and joints.

The mechanism was configured to have positive four-bar mechanism kinematics. Experimental blocked force readings were obtained by placing a force sensor at point B normal to the tip motion. Both motors were then actuated at their maximum voltage (12 V) and the output force measured. The experiment was repeated three times and each time the mechanism was released and reset to the initial position. The measured points are shown in Table 1 as the average measured experimental force. The corresponding x, y and reach (L'') are also presented in the table. Fig. 16 illustrates the positions where the measurements were taken (as indicated by numbered stars). The length (L'') is used to convert the measured force to the mechanism output torque. Each motor can generate a 95.9 mNm of stall torque and through a gearbox ratio of 66.2:1 an ideal torque of 6.35 Nm can be generated. The combined maximum torque output from the both motors is 12.7 Nm, however the maximum gearbox efficiency is rated at 70% reducing this to 8.89 Nm.

The results of the torque experiments (as presented in Table 1) illustrate that the theory predicts the mechanism output torque with 90%, or greater, accuracy. It is interesting to note that some of the experiments show a greater torque output than predicted. This implies that the stated efficiency of the gearbox is greater than the 70% quoted in the manufacturer literature and the friction within the mechanism joints is minimal; the joints all have double bearings and exhibit little friction.

3.3. Experimental trajectory tracking

A PD controller with gains of $k_p = 20$ and $k_d = 5$ was used to control the motion of the cranks to produce the desired trajectories. The measurement of the rotation of the motor link shafts were used to infer the positions of all the links. This approach is subject to measurement errors as a result of backlash effects and looseness in the joints. However, this provides a practical method of measuring the system behaviour without mounting sensors on exposed moving parts. Indeed, any slight errors that result could be compensated for by improved gearing and bearing arrangements. For this specific application tracking accuracy within $\pm 4\,mm$ was deemed acceptable.

3.3.1. Tracking the original trajectory

The original trajectory (covering the perimeter of the workspace) was implemented on the experimental system (Fig. 17). The trajectory is accurately tracked to within the desired tolerances. Around the extend and retract phases of motion there is the largest deviation from the desired trajectory – this is to be expected as joint friction effects are at their highest due to all joints of the mechanism moving. Also, the rocker arms are moving towards each other increasing the likelihood of the two PD controllers interacting (errors in the motion of one, interfere with the performance of the other).

Fig. 18 illustrates the tracking of a trajectory with reduced extension. The tracking of this trajectory is within the desired tolerance and is an improvement over the original trajectory shown

Please cite this article in press as: Richardson RC et al. The sweep-extend mechanism: A 10-bar mechanism to perform biologically inspired burrowing motions. Mechatronics (2011), doi:10.1016/j.mechatronics.2011.03.002

Table 1
Predicted and experimental output force for positive four-bar angles.

Point	x (m)	y (m)	(L'') (m)	Average exp. force (N) (three readings)	Actual output torque (Nm)	Theoretical mechanism torque ratio	Ideal output torque (Nm)	Accuracy abs (%)
1	0	0.135	0.135	51.25	7.8	0.80	7.1	91
2	0.095	0.095	0.135	54.85	7.95	0.95	8.4	91
3	0.122	0.057	0.135	56.85	8.24	0.95	8.4	98
4	0	0.085	0.085	87.4	7.4	0.78	6.9	93
5	0.6	0.6	0.085	94.01	7.99	0.95	8.4	95
6	0.31	0.87	0.085	101.65	8.6	0.95	8.4	97

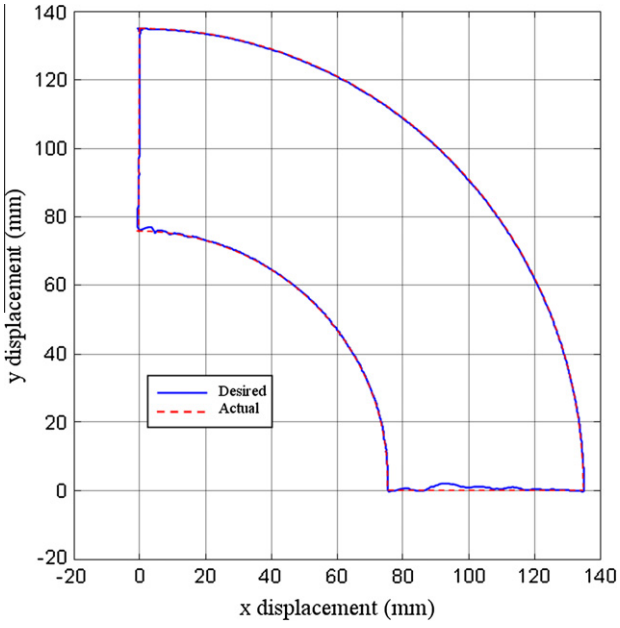

Fig. 17. Experimental tracking of original trajectory.

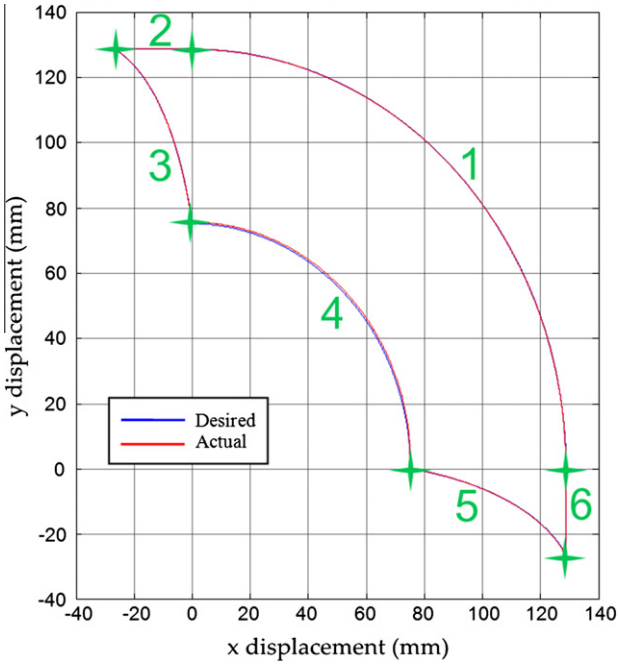

Fig. 18. Experimental tracking of trajectory with reduced extension.

in Fig. 18 due to the corner blending algorithm requiring less severe changes in extension and retraction. Labels 1–6 indicate

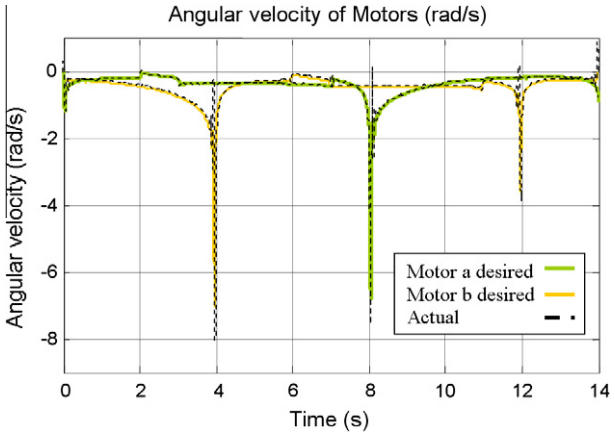

Fig. 19. Angular velocity of crank.

stages of motion shown in Fig. 20. Fig. 19 illustrates the velocity tracking of the motors during the motion of Fig. 18. The velocity is accurately tracked with acceptable oscillation at transient parts of the motion. Fig. 20 shows the tip velocity in x and y co-ordinate axis. The curved nature of the sweep and return phases of motion (labels 1 and 4 in Fig. 18) are clearly shown in Fig. 20. The return phase (4) has a lower linear x and y velocity when compared to the sweep phase (1) due to a smaller radial distance and the requirement for constant angular velocity in both phases. Curve segments 2 and 3 illustrate the constant velocity interpolation and blended motion by varying e respectively. Curve segments 5 and 6 are reflections of segments 2 and 3. Overall, the velocities are tracked well with minimal tip oscillation.

Fig. 21 illustrates the control signal for the trajectory shown in Fig. 19. At a time of 0, 4, 8 and 12 s the trajectory is at the corners of motion where the rocker link changes direction and the torque ratio is at its lowest. A small constant voltage is required to overcome friction. The control signal occasionally goes below 0 V to decelerate the crank, not to reverse its direction. Finally, Fig. 22 illustrates experimental tracking of a trajectory with greatly reduced extension within required tolerances.

4. Discussion

To fully understand the mechanism's advantages it is useful to contrast the mechanism with that of a conventional two link planar manipulator. This design would require a second motor to be mounted on a moving link, hence wasting energy to accelerate and decelerate the motor mass. Furthermore, the actuators would have to constantly change direction to implement a desired x, y co-ordinate. This constant changing direction results in wear on the bearings, electrical inefficiency, and increased tracking errors due to backlash effects. Therefore, there are clear advantages of the sweep-extend mechanism. The work has also demonstrated that the mechanism is practically feasible to create and control. This

Please cite this article in press as: Richardson RC et al. The sweep-extend mechanism: A 10-bar mechanism to perform biologically inspired burrowing motions. Mechatronics (2011), doi:10.1016/j.mechatronics.2011.03.002

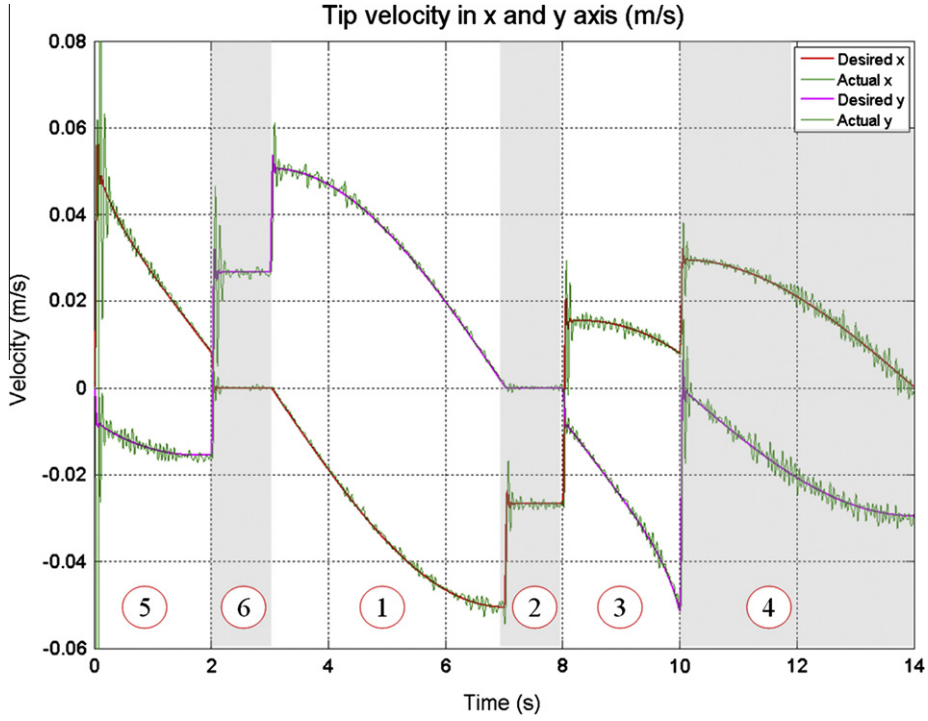

Fig. 20. Tip velocity in *x*- and *y*-axis.

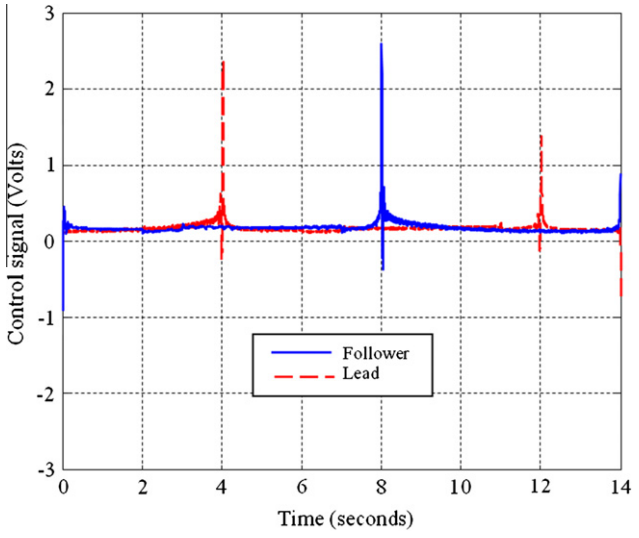

Fig. 21. Experimental control signals.

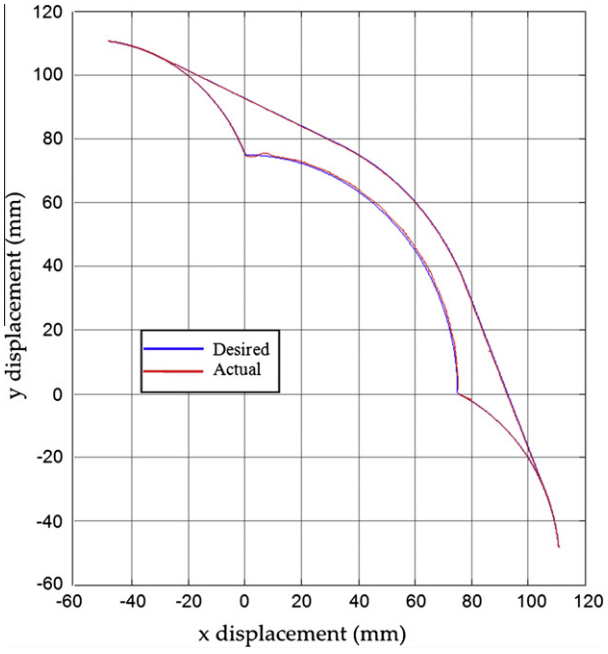

Fig. 22. Experimental tracking of significantly reduced extension.

may seem a trivial point, however it would be easy to mechanically design a mechanism that was not feasible to construct, or its behaviour was so non-linear that it was difficult to control.

The drawbacks of the mechanism are an increased number of links, resulting in the requirement of larger operational space and increased friction effects. Furthermore, closed-loop feedback control of both input cranks is required to maintain any motion; if appropriate phase differences between the rockers are not maintained, the mechanism may jam.

In spite of the drawbacks, the mechanism is a feasible method of creating controllable elliptical motions that would otherwise be difficult to produce. The electric motors used in this implementation allow forward and reverse operations. However, the potential operation of the mechanism from actuators operating in a single direction allows the use of unconventional actuators that are only capable of generating torque in a single direction.

5. Conclusions

A new type of mechanism has been designed to move an output point through a motion akin to a swimmer's breast-stroke. The analysis presented here demonstrates the mechanism is capable of a wide variety of motions. Crucially, the mechanism can be successfully physically constructed and operates as predicted by the

Please cite this article in press as: Richardson RC et al. The sweep-extend mechanism: A 10-bar mechanism to perform biologically inspired burrowing motions. Mechatronics (2011), doi:10.1016/j.mechatronics.2011.03.002

theory. Experimental tracking of desired trajectories is obtained within the desired ±4 mm threshold and the force output was within 90% of that predicted by the theory.

The analysis has highlighted some limitations in the available motions that can be implemented, whilst maintaining the movement of motor in one direction only; the most significant is a limitation on the amount of change in extend/retract direction for a given circumferential motion.

The mechanism can be used for applications where accurate control of a cyclic point motion with a movement profile similar to a swimmers breast-stroke is required. This motion has many potential application areas including burrowing robots, swimming robots, rope climbing robots and walking robots.

Acknowledgement

The authors gratefully acknowledge the support of EPSRC Grant EP/C510097/1 under which this research is being conducted.

References

[1] Murphy R. Trial by fire – activities of the rescue robots at the World Trade Centre from 11–21 September 2001. IEEE Robotics Autom Mag 2001;11(3):50–61.
[2] Gonzalez-Gomez J, Gonzalez-Quijano J, Zhang H, Abderrahim M. Towards the sense of touch in snake modular robots for search and rescue operations. ICRA; 2010.
[3] Hirose S, Yamada H. Snake-like robots. IEEE Robotics Autom Mag 2009;16(1):88–98.
[4] Masayuki A, Tanaka Y, Hirose S. Development of "Souryu-VI" and "Souryu-V:" Serially connected crawler vehicles for in-rubble searching operations. J Field Robotics 2008:31–65.
[5] Kobayashi E, Masamune K, Sakuma I, Dohi T, Hashimoto D. A new safe laparoscopic manipulator system with a five-bar linkage mechanism and an optical zoom. Comput Aided Surg 1999;4(4):182–92.
[6] Kobayashi Y, Chiyoda S, Watabe K, Okada M, Nakamura Y. Small occupancy robotic mechanisms for endoscopic surgery. Lect Notes Comput Sci 2002;2488:75–82.
[7] Minor M. Mukherjee R. A dexterous manipulator for minimally invasive surgery. In: Proceedings of 1999 IEEE international conference on robotics and automation, Detroit, MI; 1999. p. 2057–64.
[8] Degani A, Choset H, Wolf A, Zenati A. Highly Articulated robotic probe for minimally invasive surgery. In: Proceedings of the 2006 IEEE international conference on robotics and automation, Orlando, FLA; 2006. p. 4167–72.
[9] Peeters J. A SMA Actuated laparoscopic forceps with force feedback. Medical robotics, Eindhoven University of Technology/Department of Mechanical Engineering, DCT Report 2002.01; 2001.
[10] Minzhou L, Wei L, Bingyu S, Tao M. Autonomous grasping of a space robot multisensory gripper. In: Proceedings of the 2006 IEEE/RSJ International conference on intelligent robots and systems, Beijing, China; 2006. p. 1014–9.
[11] Martin T, Ambrose R, Diftler M, Platt R, and Butzer M. Tactile Gloves for Autonomous Grasping with the NASA/DARPA Robonaut. In: Proceedings of the 2004 IEEE international conference on robotics and automation, New Orleans, LA; 2004. p. 1713–8.
[12] Thueer T, Krebs A, Siegwart R. Comprehensive locomotion performance evaluation of all-terrain robots. In: Proceedings of the 2006 IEEE/RSJ international conference on intelligent robots and systems, Beijing, China; 2006. p. 4260–5.
[13] Feliu V, Garcia A, Somolinos J. Gauge-based tip position control of a new three-degree-of-freedom flexible robot. J Robotics Res 2001;20(8):660–75.
[14] Figliolini G, Ceccarelli M. EP-WAR3 biped robot for climbing and descending stairs. Robotica 2004;22(4):405–17.
[15] Pons J, Ceres R, Jimenez A. Mechanical design of a fruit picking manipulator: improvement of dynamic behavior. In: Proceedings of the 1996 IEEE international conference on robotics and automation, Minneapolis, Minnesota, April 1996. p. 969–74.
[16] Zhixing W, Hongying W, Dewei T, Jiansheng L. Study on rigid-body guidance synthesis of planar linkage. Mech Mach Theory 2002;37:673–84.
[17] Marble SD, Pennock GR. Algebraic–geometric properties of the coupler curves of the RCCC spatial four-bar mechanism. Mech Mach Theory 2000;35:675–93.
[18] Scott R, Richardson R. A novel USAR Digging Mechanism. In: Proceedings of the 2006 IEEE/RSJ international conference on intelligent robots and systems, Beijing, China; 2006. p. 3498–503.
[19] Scott R, Richardson R. Realities of biologically inspired design with a subterranean digging robot example. In: Proceedings of IASTED international conference on robotics and applications, Cambridge, USA; 2005.
[20] Sclater N, Chironis N. Mechanisms and mechanical devices sourcebook. McGraw-Hill. ISBN 978007146761.
[21] Oziegbe-orhuwa P, Odiase Scott R, Richardson R. A haptic object probe with Urban Search and Rescue applications. In: IEEE international workshop on safety, security and rescue robotics. August 22–24. Gaithersburg, MD, USA; 2006.
[22] Shigley JE, Uicker Jr JJ. Theory of machines and mechanisms. New York: McGraw-Hill; 2003, ISBN 978-0195155983.
[23] Craig J. Introduction to robotics: mechanics and control. Prentice Hall; 2004. ISBN 0131236296.

Please cite this article in press as: Richardson RC et al. The sweep-extend mechanism: A 10-bar mechanism to perform biologically inspired burrowing motions. Mechatronics (2011), doi:10.1016/j.mechatronics.2011.03.002